IJE TRANSACTIONS A: Basics Vol. 26, No. 4, (April 2013) 447-454

International Journal of Engineering

Journal Homepage: www.ije.ir

RESEARCH NOTE

Validation of Shell Theory for Modeling the Radial Breathing Mode of a Single-Walled Carbon Nanotube

S. Basirjafari [a], S. Esmaielzadeh Khadem [*b], R. Malekfar [a]

[a] *Department of Physics, Tarbiat Modares University, P.O. Box 14115-175, Tehran, I.R. Iran*

[b] *Department of Mechanical and Aerospace Engineering, Tarbiat Modares University, P.O. Box 14115-177, Tehran, I.R. Iran*

PAPER INFO

Paper history:
Received 14 November 2011
Received in revised form 21 October 2012
Accepted 15 November 2012

Keywords:
Analytical Solution
Elastic Thin Shell Theory
Hamilton's Principle
Radial Breathing Mode (RBM) Frequency
Single-Walled Carbon Nanotube (SWCNT)

ABSTRACT

In this paper, the radial breathing mode (RBM) frequency of single-walled carbon nanotube (SWCNT) is studied based on the thin shell theory. For this purpose, SWCNT is considered as an elastic thin cylindrical shell. The dynamic equation of RBM is derived using the Hamilton's principle. An analytical solution of the RBM frequency of SWCNT is obtained. The advantage of this formulation is that it shows the dependency of the RBM frequency to the mechanical properties of SWCNT, clearly. These investigations are very important to predict the accurate vibrational characteristics of SWCNTs which have potential applications in nanotube-filled nanocomposites that are used as sound absorbers. To show the accuracy of this work, the RBM frequencies of 40 different SWCNTs are obtained which are in excellent agreement with the available experimental results with relative errors less than 1%. Also, the RBM frequencies predicted by the present shell model are compared with those obtained by the other researchers based on the density-functional theory (DFT), and three-dimensional (3D) elasticity theory. The results emphasize the utility of thin shell theory for modeling and vibrational behavior of the RBM frequency of SWCNT.

doi: *10.5829/idosi.ije.2013.26.04a.13*

1. INTRODUCTION

Carbon nanotubes (CNTs) with unique stiffness, strength and low density could influentially affect some of the physical properties of composites filled with CNTs for sound wave absorption [1, 2] or being used as sensors and actuators [3]. It is clear that the effective properties of CNT-based nanocomposites depend on properties of individual components. They have superior physical and mechanical properties, compared with bulk materials. So, the study on vibrational characteristics of individual CNTs with appropriate model is very important for designing CNT-based nanocomposites such as sound absorbers [1, 2], and nano-devices such as advanced miniaturized switches [4].

Many of SWCNT properties have been studied experimentally [5-7], and theoretically [8-15]. Raman spectroscopy has provided an extremely powerful tool for the characterization of SWCNT. The RBM frequency is usually the strongest feature in SWCNT Raman spectra plays a crucial role in the experimental determination of the geometrical properties of SWCNTs. Therefore, it is very important to know the behavior of RBM frequency of different nanotubes, precisely. The aim of this paper is only the prediction of the RBM frequencies. In the RBM, all carbon atoms move coherently in the radial direction creating a breathing-like vibration of the entire tube. This feature is specific to CNTs and does not exist in graphite [16]. Therefore, RBM frequencies are very useful for identifying a given material containing SWCNTs, through the existence of RBM modes, and for characterizing the nanotube diameter distribution in the sample through inverse proportionality of the RBM frequency to the tube diameter.

A SWCNT can be described as a single layer of a graphite crystal that is rolled up into a seamless circular cylinder, one atom thickness, usually with a small number of carbon atoms along the circumference and a long length along the cylinder axis.

Owing to nanometer dimensions of CNTs, it is difficult to set up controlled experiments to measure the

*Corresponding Author Email: khadem@modares.ac.ir (S. Esmaielzadeh Khadem)

properties of an individual CNT [5-7]. Also, molecular-dynamics and atomistic methods such as density-functional theory (DFT) [8-10] are costly and difficult particularly for large-scale systems. So, continuum elastic mechanical models such as elastic beam models [11, 12] and elastic shell models [13, 14] have been widely used to study vibration of CNTs.

In this paper, SWCNT is modeled as an elastic thin cylindrical shell. Afterwards, the dynamic equations of motion are derived according to the first approximation thin shell theory. Then, closed form solution for RBM frequency of SWCNT is obtained. Finally, the RBM frequencies of 40 different SWCNTs are compared with the available experimental results [5-7] which show an excellent agreement with relative errors of less than 1%. The results show more agreement with the experimental results [5-7] than the DFT results [8-10] and Mahan's three-dimensional (3D) elasticity theory [15].

2. MODELING THE SWCNT

In this study, the SWCNT is modeled as an elastic thin circular cylindrical shell with radius R and thickness h, in cylindrical coordinates (r,θ,x) as shown in Figure 1, where r, θ and x are the radial, circumferential and axial coordinates of the cylindrical shell, respectively. In Figure 1, u, v and w are the shell displacements along the axial, circumferential and radial directions, respectively.

According to the first approximation thin shell theory [17], the stress-strain relations for a three-dimensional element of the shell are as follows:

$$\sigma_x = \frac{E}{1-\mu^2}\left\{\frac{\partial u}{\partial x} - z\frac{\partial^2 w}{\partial x^2} + \mu\left[\frac{1}{R}\left(w+\frac{\partial v}{\partial \theta}\right) + z\frac{1}{R^2}\left(\frac{\partial v}{\partial \theta} - \frac{\partial^2 w}{\partial \theta^2}\right)\right]\right\},$$
$$\sigma_\theta = \frac{E}{1-\mu^2}\left[\frac{1}{R}\left(w+\frac{\partial v}{\partial \theta}\right) + z\frac{1}{R^2}\left(\frac{\partial v}{\partial \theta} - \frac{\partial^2 w}{\partial \theta^2}\right) + \mu\left(\frac{\partial u}{\partial x} - z\frac{\partial^2 w}{\partial x^2}\right)\right], \quad (1)$$
$$\sigma_{x\theta} = \frac{E}{2(1+\mu)}\left[\frac{\partial v}{\partial x} + \frac{1}{R}\frac{\partial u}{\partial \theta} + z\frac{2}{R}\left(\frac{\partial v}{\partial x} - \frac{\partial^2 w}{\partial x \partial \theta}\right)\right],$$

where E and μ are the elastic modulus and Poisson's ratio of SWCNT, respectively. The normal stress σ_z which acts in the normal direction to the middle surface of the shell is neglected. Although, the transverse shear deflections γ_{xz} and $\gamma_{\theta z}$ are assumed to be negligible, one may not neglect the integrated effect of the transverse shear stresses σ_{xz} and $\sigma_{\theta z}$ for obtaining the transverse shear forces Q_x and Q_θ acting at the normal direction to the middle surface of the shell. By integrating the stresses across the thickness h of the shell, the resultant forces N_x, N_θ, Q_x, Q_θ, $N_{x\theta}$, and $N_{\theta x}$ of the middle surface (Figure 2(a)) are [17]:

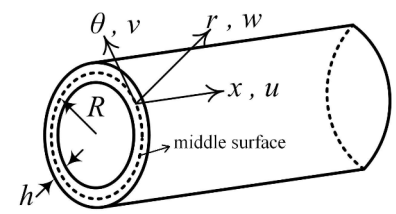

Figure 1. Cylindrical coordinates

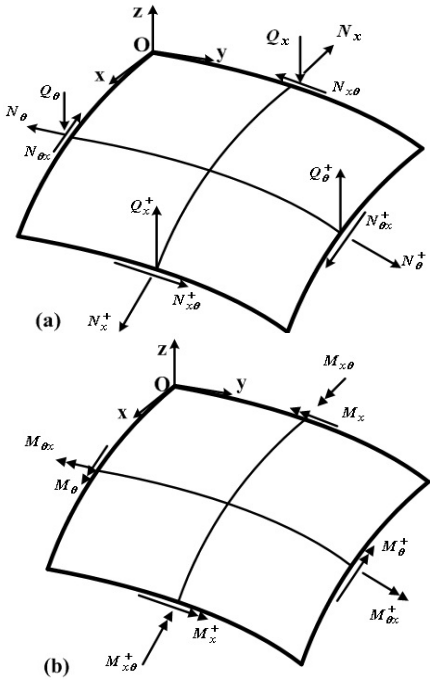

Figure 2. (a) Resultant forces and **(b)** resultant moments in cylindrical coordinates

$$\begin{Bmatrix} N_x \\ N_\theta \\ N_{x\theta} \\ N_{\theta x} \\ Q_x \\ Q_\theta \end{Bmatrix} = \int_{-h/2}^{h/2} \begin{Bmatrix} \sigma_x \\ \sigma_\theta \\ \sigma_{x\theta} \\ \sigma_{\theta x} \\ \sigma_{xz} \\ \sigma_{\theta z} \end{Bmatrix} \mathrm{d}z, \quad (2)$$

and the resultant moments M_x, M_θ, $M_{x\theta}$ and $M_{\theta x}$ exerted on the middle surface (see Figure 2(b)) can be obtained as [17]:

$$\begin{Bmatrix} M_x \\ M_\theta \\ M_{x\theta} \\ M_{\theta x} \end{Bmatrix} = \int_{-h/2}^{h/2} \begin{Bmatrix} \sigma_x \\ \sigma_\theta \\ \sigma_{x\theta} \\ \sigma_{\theta x} \end{Bmatrix} z\,\mathrm{d}z. \quad (3)$$

From the theory of elasticity, by integrating the strain energy stored in one infinitesimal element of the shell volume, the strain energy stored in the shell is

given by [17]:

$$U = \frac{1}{2}\iiint_V \left(\sigma_x e_x + \sigma_\theta e_\theta + \sigma_{x\theta} e_{x\theta} + \sigma_{xz}\gamma_{xz} + \sigma_{\theta z}\gamma_{\theta z}\right) R \, \mathrm{d}x \, \mathrm{d}\theta \, \mathrm{d}z. \quad (4)$$

Integrating over the thickness of the shell ($z=-h/2$ to $h/2$), the kinetic energy of the shell is obtained as [17]:

$$\mathrm{K} = \frac{1}{2}\rho h \int_x \int_\theta \left[\dot{u}^2 + \dot{v}^2 + \dot{w}^2 + \frac{h^2}{12}\left(\dot{\beta}_x^2 + \dot{\beta}_\theta^2\right)\right] R \, \mathrm{d}x \, \mathrm{d}\theta, \quad (5)$$

where ρ is the shell mass density, β_x and β_θ represent rotations in the normal directions to the middle surface about x and θ axes, respectively, and dot indicates a time derivative.

The variation of energy of the shell due to applied boundary forces and the resultant moments are [17]:

$$\begin{aligned}\delta E_{\mathrm{B}} = &\int_x \left(N_\theta \delta v + N_{\theta x}\delta u + Q_\theta \delta w + M_\theta \delta\beta_\theta + M_{\theta x}\delta\beta_x\right)\mathrm{d}x \\ &+ \int_\theta \left(N_x \delta u + N_{x\theta}\delta v + Q_x \delta w + M_x \delta\beta_x + M_{x\theta}\delta\beta_\theta\right) R \, \mathrm{d}\theta.\end{aligned} \quad (6)$$

The symbol δ is the variational symbol and is treated mathematically as a differential symbol.
The Hamilton's principle is expressed as [17]:

$$\delta \int_{t_0}^{t_1} (U - \mathrm{K} - E_{\mathrm{B}}) \, \mathrm{d}t = 0, \quad (7)$$

at arbitrary times t_0 and t_1, all variations are zero including the variational displacements. By substituting Equations (4)-(6) into Equation (7) and taking the variational operator inside the integral, one obtains:

$$\begin{aligned}\int_{t_0}^{t_1}\int_x\int_\theta \Bigg\{ &\left[R\frac{\partial N_x}{\partial x} + \frac{\partial N_{\theta x}}{\partial \theta} - \rho h R \frac{\partial^2 u}{\partial t^2}\right]\delta u \\ &+ \left[R\frac{\partial N_{x\theta}}{\partial x} + \frac{\partial N_\theta}{\partial \theta} + Q_\theta - \rho h R \frac{\partial^2 v}{\partial t^2}\right]\delta v \\ &+ \left[R\frac{\partial Q_x}{\partial x} + \frac{\partial Q_\theta}{\partial \theta} - N_\theta - \rho h R \frac{\partial^2 w}{\partial t^2}\right]\delta w \\ &+ \left[R\frac{\partial M_x}{\partial x} - Q_x R + \frac{\partial M_{\theta x}}{\partial \theta}\right]\delta\beta_x \\ &+ \left[R\frac{\partial M_{x\theta}}{\partial x} - Q_\theta R + \frac{\partial M_\theta}{\partial \theta}\right]\delta\beta_\theta \Bigg\} \times \mathrm{d}x \, \mathrm{d}\theta \, \mathrm{d}t = 0.\end{aligned} \quad (8)$$

In order to satisfy this equation, every individual of the triple integral parts must be equal to zero. Moreover, because of the arbitrary variational displacements, each integral equation can be satisfied only if the coefficients of the variational displacements are zero. So, one obtains the following equations that are called "Love's equations":

$$R\frac{\partial N_x}{\partial x} + \frac{\partial N_{\theta x}}{\partial \theta} - \rho h R \frac{\partial^2 u}{\partial t^2} = 0 \quad (9)$$

$$R\frac{\partial N_{x\theta}}{\partial x} + \frac{\partial N_\theta}{\partial \theta} + Q_\theta - \rho h R \frac{\partial^2 v}{\partial t^2} = 0 \quad (10)$$

$$R\frac{\partial Q_x}{\partial x} + \frac{\partial Q_\theta}{\partial \theta} - N_\theta - \rho h R \frac{\partial^2 w}{\partial t^2} = 0 \quad (11)$$

$$R\frac{\partial M_x}{\partial x} - Q_x R + \frac{\partial M_{\theta x}}{\partial \theta} = 0 \quad (12)$$

$$R\frac{\partial M_{x\theta}}{\partial x} - Q_\theta R + \frac{\partial M_\theta}{\partial \theta} = 0 \quad (13)$$

In the RBM vibration, all carbon atoms move in phase in the radial direction creating a breathing-like vibration of the entire tube. Therefore, the RBM vibration is axi-symmetric for the entire tube (e. g. $\partial/\partial\theta = 0$ and $\partial/\partial x = 0$).
So, the Love's equations reduce to:

$$N_\theta + \rho h R \frac{\partial^2 w}{\partial t^2} = 0 \quad (14)$$

By substituting σ_θ from Equation (1) into Equation (2) with the mentioned assumptions, $\partial/\partial\theta = 0$ and $\partial/\partial x = 0$, the in-plane membrane force of the middle surface can be obtained as:

$$N_\theta = \frac{Eh}{(1-\mu^2)}\frac{w}{R}. \quad (15)$$

Substituting Equation (15) into Equation (14) gives the dynamic governing equation for the RBM vibration of SWCNT as:

$$\frac{Eh}{(1-\mu^2)}\frac{1}{R^2}w + \rho h \frac{\partial^2 w}{\partial t^2} = 0, \quad (16)$$

The RBM displacement of the SWCNT is of the form $w = W\exp(-i\omega t)$, where W is the radial displacement amplitude of the SWCNT and ω is the angular frequency of the RBM. Substituting the RBM displacement into Equation (16), gives the characteristic polynomial in terms of ω. By solving the characteristic polynomial equation, one can yield:

$$\omega = \frac{1}{R}\sqrt{\frac{E}{\rho(1-\mu^2)}}, \quad (17)$$

Experimentally, the RBM frequency is related to ω via $f_{\mathrm{RBM}} = \omega/2\pi C$ where $C = 2.99792458\times10^8$ m/s [18] is the velocity of light.
So, the RBM frequency formula can be obtained as:

$$f_{\mathrm{RBM}} = \frac{1}{\pi C}\sqrt{\frac{E}{\rho(1-\mu^2)}}.\frac{1}{2R}, \quad (18)$$

Throughout the paper, the material properties of SWCNT have been considered as: Young's modulus E=1 TPa, mass density ρ=2300 kg/m^3 [12] and Poisson's ratio μ=0.2 [14]. Each SWCNT is uniquely specified by the two chiral indices, n and m ($n \geq m$), which are the two integer coefficients in the expression of the chiral vector which is often described by the

pair of indices (n,m). The diameter of the SWCNT (n,m) is given by [16]:

$$d = 2R = \frac{a_0}{\pi}\sqrt{3\left(n^2 + nm + m^2\right)}, \quad (19)$$

where the value a_0=1.421 Å has been used for the carbon-carbon (C-C) bond length [7].

The advantage of the simple analytical formula (18) is that it shows clearly the dependency of the constant A in $f_{RBM} = A/d$ to the mechanical properties of SWCNT as:

$$A = \frac{1}{\pi C}\sqrt{\frac{E}{\rho\left(1-\mu^2\right)}}. \quad (20)$$

3. INFLUENCE OF CHANGING THE MECHANICAL PROPERTIES OF SWCNT (10, 10) ON ITS RBM FREQUENCY

In this section, the influence of changing the mechanical parameters of a SWCNT (10,10) with radius R=0.678 nm on its RBM frequency has been investigated.

Figure 3 shows that by increasing the Young's modulus, E, of SWCNT, the RBM frequency increases.

Figure 4 shows that the RBM frequency of SWCNT decreases with an increase in the mass density, ρ, of SWCNT.

Figure 5 shows the influence of the Poisson's ratio of SWCNT on its RBM frequency. The RBM frequency of SWCNT is approximately insensitive to its Poisson's ratio. Figure 5 shows that the RBM frequency of SWCNT increases with an increase in its Poisson's ratio, very slowly.

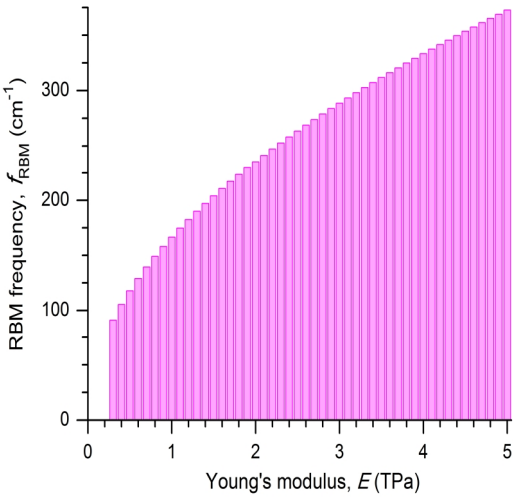

Figure 3. The RBM frequency of SWCNT (10,10) versus its Young's modulus, E (TPa)

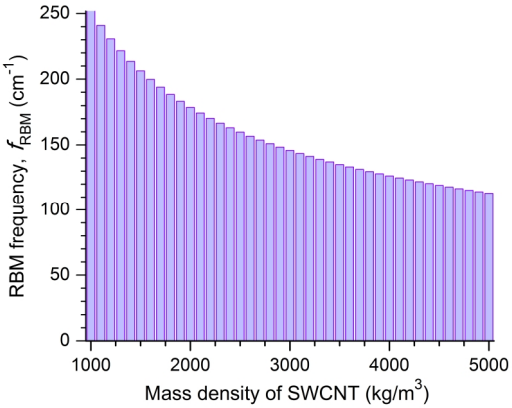

Figure 4. The RBM frequency of SWCNT (10,10) versus its mass density, ρ (kg/m^3)

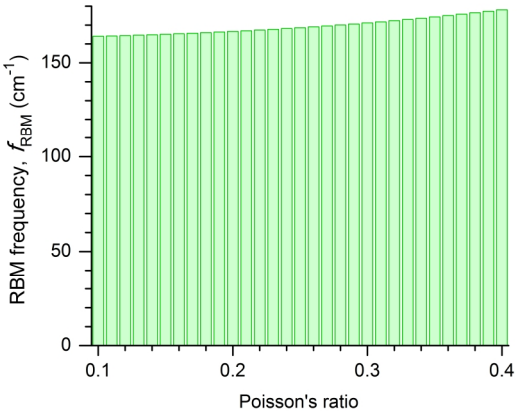

Figure 5. The RBM frequency of SWCNT (10,10) versus its Poisson's ratio, μ

4. VALIDATION OF THIN SHELL THEORY FOR MODELING THE RBM FREQUENCY OF SWCNT IN COMPARISON WITH OTHER THEORETICAL MODELS

Substituting the material properties of SWCNT into Equation (18), gives the RBM frequency as f_{RBM}=226 cm^{-1} (nm/d) which is in good agreement with the experimental results 223.5 cm^{-1} (nm/d) [5], 223.75 cm^{-1} (nm/d) [6] and 224 cm^{-1} (nm/d) [7]. Some researchers have obtained different values as: 232 cm^{-1} (nm/d) [8] and 234 cm^{-1} (nm/d) [9] based on the local-density approximation (LDA) with respect to DFT, and 227 cm^{-1} (nm/d) based on Mahan's 3D elasticity theory [15]. Therefore, it can be concluded that the results of this paper are in good agreement with the experimental results compared to the DFT and Mahan's 3D elasticity theory results.

Table 1 shows the RBM frequencies of 40 different SWCNTs in comparison with the available experimental and atomic results. The first two columns show the n and

TABLE 1. Comparison between the results obtained in this work and the available experimental results [5-7], the other theoretical results based on DFT [8-10], and Mahan's three-dimensional elasticity theory [15] all in cm^{-1}. All errors (%) have been computed relative to the average values of experimental results (e. g. f_{RBM}=223.75 [6] cm^{-1} (nm/d))

n	m	d (nm)	Experimental results			Theoretical results							
			Ref. [5]	Ref. [6]	Ref. [7]	Ref. [8], error ≈ 3.7%	Ref. [9], error ≈ 4.6%	DFT [10]	error (%)	DFT* [10]	error (%)	Ref. [15], error ≈ 1.5%	This work error ≈ 1%
4	0	0.3132	713.6	714.4	715.2	740.7	747.1	651.3	8.8	642.3	10.1	724.8	721.4
3	2	0.3413	654.8	655.6	656.3	679.8	685.6	651.1	0.7	648.6	1.1	665.1	662.0
4	1	0.3588	622.9	623.6	624.3	646.6	652.2	589.5	5.5	584.1	6.3	632.7	629.7
5	0	0.3915	570.9	571.5	572.2	592.6	597.7	544.9	4.7	536.1	6.2	579.8	577.1
3	3	0.4069	549.3	549.9	550.5	570.2	575.1	541.1	1.6	551.4	0.3	557.9	555.3
4	2	0.4143	539.5	540.1	540.7	160.0	564.8	539.5	0.1	536.3	0.7	547.9	545.3
5	1	0.4360	512.6	513.2	513.8	532.1	536.7	487.1	5.1	493.2	3.9	520.6	518.3
6	0	0.4698	475.7	476.3	476.8	493.8	498.1	463.6	2.7	458.5	3.7	483.2	480.9
4	3	0.4763	469.2	469.8	470.3	487.1	491.3	479.4	2.1	476.0	1.3	476.6	474.4
5	2	0.4890	457.1	457.6	458.1	474.4	478.5	451.5	1.3	448.8	1.9	464.2	462.1
6	1	0.5135	435.2	435.7	436.2	451.8	455.7	437.8	0.5	432.8	0.7	442.1	440.1
4	4	0.5425	412.0	412.4	412.9	427.6	431.3	424.3	2.9	419.2	1.6	418.4	416.5
5	3	0.5481	407.8	408.2	408.7	423.3	426.9	417.4	2.2	413.5	1.3	414.2	412.2
7	0	0.5481	407.8	408.2	408.7	423.3	426.9	411.0	0.7	405.3	0.7	414.2	412.2
6	2	0.5647	395.8	396.2	396.7	410.8	414.4	404.5	2.1	400.2	1.0	402.0	400.2
7	1	0.5912	378.0	378.5	378.9	392.4	395.8	374.6	1.0	373.1	1.4	384.0	382.2
6	3	0.6215	359.6	360.0	360.4	373.3	376.5	364.5	1.2	363.1	0.9	365.2	363.6
8	0	0.6264	356.8	357.2	357.6	370. 4	373.6	363.6	1.8	358.5	0.4	362.4	360.7
5	5	0.6781	329.6	330.0	330.3	342.1	345.1	337.3	2.2	338.9	2.7	334.8	333.2
6	4	0.6826	327.4	327. 8	328.2	339.9	342.8	336.1	2.5	333.4	1.7	332.6	331.0
9	0	0.7047	317.2	317.5	317.9	329.2	332.1	317.8	0.1	318.2	0.2	322.1	320.6
8	2	0.7177	311.4	311.8	312.1	323.3	326.0	316.5	1.5	314.9	1.0	316.3	314.9
7	4	0.7551	296.0	296.3	296.6	307.2	309.9	307.1	3.6	303.7	2.5	300.6	299.2
10	0	0.7830	285.4	285.8	286.1	296.3	298.9	294.5	3.1	290.7	1.7	289.9	288.6
6	6	0.8138	274.6	274.9	275.3	285.1	287.5	284.3	3.4	283.6	3.1	278.9	277.7
11	0	0.8613	259.5	259.8	260.1	269.4	271.7	268.2	3.2	264.6	1.9	263.6	262.3
12	0	0.9397	237.8	238.1	238.4	246.9	249.0	242.8	2.0	242.2	1.7	241.6	240.5
7	7	0.9494	235.4	235.7	235.9	244.4	246.5	246.2	4.5	243.4	3.3	239.1	238.0
13	0	1.0180	219.5	219.8	220.0	227.9	229.9	228.9	4.1	225.5	2.6	223.0	222.0
8	8	1.0850	206.0	206.2	206.5	213.8	215.7	216.5	5.0	213.1	3.3	209.2	208.3
14	0	1.0963	203.9	204.1	204.3	211.6	213.4	212.4	4.1	209.7	2.7	207.1	206.1
15	0	1.1746	190.3	190.5	190.7	197.5	199.2	196.4	3.1	195.6	2.7	193.3	192.4
9	9	1.2206	183.1	183.3	183.5	190.1	191.7	192.7	5.1	189.4	3.3	186.0	185.1
16	0	1.2529	178.4	178.6	178.8	185.2	186.8	186.4	4.4	183.7	2.9	181.2	180.4
17	0	1.3312	167.9	168.1	168.3	174.3	175.8	175.6	4.5	173.0	2.9	170.5	169.7
10	10	1.3563	164.8	165.0	165. 2	171.1	172.5	173.6	5.2	170.7	3.5	167.4	166.6
18	0	1.4095	158.6	158.7	158.9	164.6	166.0	164.4	3.6	163.5	3.0	161.1	160.3
19	0	1.4878	150.2	150.4	150.6	155.9	157.3	157.3	4.6	155.1	3.1	152.6	151.9
11	11	1.4919	149.8	150.0	150.1	155.5	156.8	158.0	5.3	155.2	3.5	152.2	151.5
20	0	1.5661	142.7	142.9	143.0	148.1	149.4	149.3	4.5	147.1	3.0	144.9	144.3

m chiral indices; the third column shows the SWCNT diameter (*d*, in nm) from Equation (19) and the next three columns are the experimental results. Afterwards, the next six columns show the results obtained based on DFT, and the error percentages of DFT and DFT* in comparison with the experimental results.

DFT assumes that all carbon atoms move purely in a radial direction, and DFT* assumes coupling with the totally symmetric tangential modes [10]. The next column shows the results obtained by Mahan's 3D elasticity [15]. The last column shows the results of this work obtained based on thin shell theory.

From Table 1, it could be concluded that the present paper, using the thin shell theory, could predict the RBM frequencies of different SWCNTs in good agreement with the available experimental results [5-7] with relative errors of less than 1%.

Figure 6 shows the influence of changing the radius of SWCNT on its RBM frequency.

As it is shown in Figure 6, the RBM frequency is very sensitive to the radius, *R*, of SWCNT when this geometrical property is extremely small. The RBM frequency decreases strongly with increasing the radius of SWCNT, in the range of less than 1.5 nm, then it tends to a constant value. The accuracy of this frequency-radius relation has been shown in Table 1. The product of the RBM frequency and the SWCNT diameter in cm^{-1} nm has been illustrated in Figure 7. Figure 7, provides a better illustration of comparison between the RBM frequencies obtained in the present paper based on thin shell theory and the available different experimental results [5-7], and the other theories [8-10,15]. The lowermost three lines show the experimental results [5-7] that are around 223.75 cm^{-1} nm, very close to each other. The upper dot line is the results obtained in the present paper. This is in good agreement with the experimental results with relative errors less than 1%. The next upper dash-double dot line is obtained by Mahan's 3D elasticity theory [15] that is close to this paper results. The uppermost two lines show the results obtained based on the LDA with respect to DFT [8,9]. The open square and the solid circles symbols show the results obtained by Kurti et al. [10]. They have studied theoretically the RBM of SWCNTs by using the LDA with respect to DFT by the projector augmented-wave (PAW) method.

To obtain the open square results, Kürti et al. [10] assumed that all carbon atoms move purely in a radial direction. To obtain the solid circle results, they assumed the coupling of the RBM to the totally symmetric tangential modes

As it is shown in Figure 7, the results obtained by Kürti et al. [10] do not follow a simple ratio, *A/d*, behavior. The deviation of their results from the ideal behavior increases with decreasing the diameter of the SWCNT.

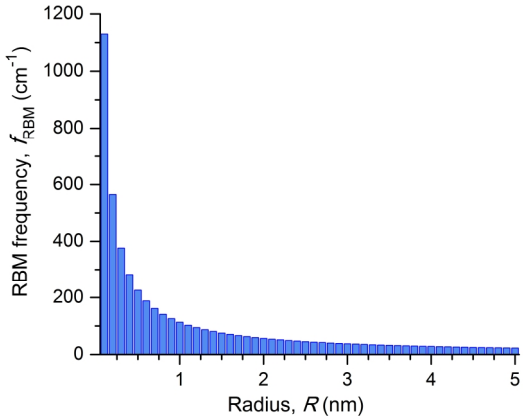

Figure 6. The RBM frequency of SWCNT versus its radius, *R* (nm)

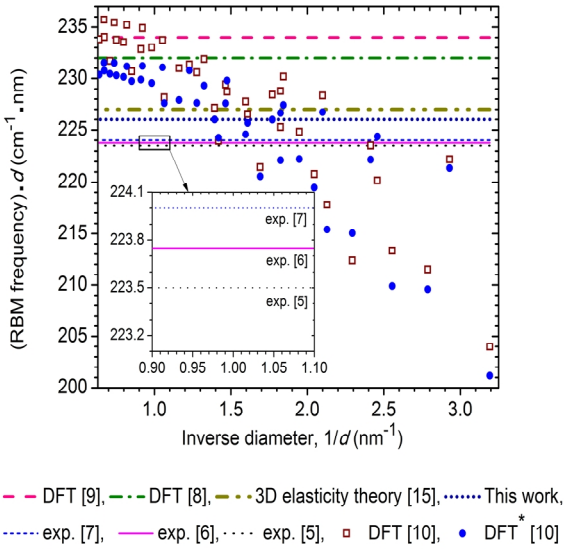

Figure 7. The product of the RBM frequency and the SWCNT diameter in cm^{-1} nm versus the inverse diameter (nm^{-1})

5. CONCLUSIONS

This paper provides a detailed investigation on the RBM frequency of the SWCNT based on the elastic thin shell theory. The following points can be concluded:

- An analytical solution of the RBM frequency of SWCNT is obtained. The advantage of this simple formula is that it shows the dependency of the RBM frequency to the mechanical properties of SWCNT, clearly.
- The simple formula for the RBM frequency of SWCNT shows that by increasing the Young's modulus (E) and the Poisson's ratio (μ) of the SWCNT, its RBM frequency increases; however by increasing the mass density (ρ) and the radius (R), its RBM frequency decreases.

- The RBM frequencies of 40 different SWCNTs are obtained which are in excellent agreement with the available experimental results with relative errors of less than 1%.
- The RBM frequencies predicted by the present shell model have been compared with those obtained by the other researchers based on the density-functional theory (DFT), and Mahan's 3D elasticity theory. The results precisely emphasize the utility of thin shell theory for modeling the RBM vibrational behavior of SWCNTs.

6. REFERENCES

1. Verdejo, R., Stämpfli, R., Alvarez-Lainez, M., Mourad, S., Rodriguez-Perez, M., Brühwiler, P., and Shaffer, M., "Enhanced acoustic damping in flexible polyurethane foams filled with carbon nanotubes", ***Composites Science and Technology***, Vol. 69, No. 10, (2009), 1564-1569.
2. Bian, Z., Wang, R. J., Zhao, D. Q., Pan, M. X., Wang, Z. X., and Wang, W. H., "Excellent ultrasonic absorption ability of carbon-nanotube-reinforced bulk metallic glass composites", ***Applied physics letters***, Vol. 82, No. 17, (2003), 2790-2792.
3. Wang, C., Li, L. and Chew, Z., "Vibrating zno–cnt nanotubes as pressure/stress sensors", ***Physica E: Low-dimensional Systems and Nanostructures***, Vol. 43, No. 6, (2011), 1288-1293.
4. Rasekh, M., Khadem, S. and Tatari, M., "Nonlinear behaviour of electrostatically actuated carbon nanotube-based devices", ***Journal of Physics D: Applied Physics***, Vol. 43, No. 31, (2010), 315301.
5. Bachilo, S. M., Strano, M. S., Kittrell, C., Hauge, R. H., Smalley, R. E., and Weisman, R. B., "Structure-assigned optical spectra of single-walled carbon nanotubes", ***Science***, Vol. 298, No. 5602, (2002), 2361-2366.
6. Rao, A., Richter, E., Bandow, S., Chase, B., Eklund, P., Williams, K., Fang, S., Subbaswamy, K., Menon, M., and Thess, A., "Diameter-selective raman scattering from vibrational modes in carbon nanotubes", ***Science***, Vol. 275, No. 5297, (1997), 187-191.
7. Bandow, S., Asaka, S., Saito, Y., Rao, A., Grigorian, L., Richter, E., and Eklund, P., "Effect of the growth temperature on the diameter distribution and chirality of single-wall carbon nanotubes", ***Physical Review Letters***, Vol. 80, No. 17, (1998), 3779-3782.
8. Sánchez-Portal, D., Artacho, E., Soler, J. M., Rubio, A. and Ordejón, P., "Ab initio structural, elastic, and vibrational properties of carbon nanotubes", ***Physical Review B***, Vol. 59, No. 19, (1999), 12678.
9. Kürti, J., Kresse, G. and Kuzmany, H., "First-principles calculations of the radial breathing mode of single-wall carbon nanotubes", ***Physical Review B***, Vol. 58, No. 14, (1998), 8869-8872.
10. Kürti, J., Zólyomi, V., Kertesz, M. and Sun, G., "The geometry and the radial breathing mode of carbon nanotubes: Beyond the ideal behaviour", ***New Journal of Physics***, Vol. 5, No. 1, (2003), 125.
11. Heireche, H., Tounsi, A., Benzair, A., Maachou, M. and Adda Bedia, E., "Sound wave propagation in single-walled carbon nanotubes using nonlocal elasticity", ***Physica E: Low-dimensional Systems and Nanostructures***, Vol. 40, No. 8, (2008), 2791-2799.
12. Yoon, J., Ru, C. and Mioduchowski, A., "Flow-induced flutter instability of cantilever carbon nanotubes", ***International journal of solids and structures***, Vol. 43, No. 11, (2006), 3337-3349.
13. Hoseinzadeh, M. and Khadem, S., "Thermoelastic vibration and damping analysis of double-walled carbon nanotubes based on shell theory", ***Physica E: Low-dimensional Systems and Nanostructures***, Vol. 43, No. 6, (2011), 1146-1154.
14. Xu, C. and Wang, X., "Matrix effects on the breathing modes of multiwall carbon nanotubes", ***Composite structures***, Vol. 80, No. 1, (2007), 73-81.
15. Mahan, G., "Oscillations of a thin hollow cylinder: Carbon nanotubes", ***Physical review B. Condensed matter and materials physics***, Vol. 65, No. 23, (2002), 235402.1-235402.7.
16. Thomsen, C., Reich, S. and Maultzsch, J., *Carbon nanotubes: Basic concepts and physical properties*. 2004, Wiley-VCH.
17. Soedel, W. and Qatu, M. S., "Vibrations of shells and plates", ***The Journal of the Acoustical Society of America***, Vol. 117, No. 4, (2005), 1683-1683.
18. Daintith, J., "The facts on file dictionary of physics", Infobase Publishing, (2009).

Validation of Shell Theory for Modeling the Radial Breathing Mode of a Single-Walled Carbon Nanotube

RESEARCH NOTE

S. Basirjafari [a], S. Esmaielzadeh Khadem [b], R. Malekfar [a]

[a] *Department of Physics, Tarbiat Modares University, Tehran, Iran*

[b] *Department of Mechanical and Aerospace Engineering, Tarbiat Modares University, Tehran, Iran*

P A P E R I N F O

Paper history:
Received 14 November 2011
Received in revised form 21 October 2012
Accepted 15 November 2012

Keywords:
Analytical Solution
Elastic Thin Shell Theory
Hamilton's Principle
Radial Breathing Mode (RBM) Frequency
Single-Walled Carbon Nanotube (SWCNT)

چکیده

در این مقاله، بسامد مُد تنفسی شعاعیِ نانولوله‌کربنی تک‌لایه بر اساس نظریه پوسته نازک مطالعه شده است. برای این منظور، نانولوله‌کربنی تک‌لایه به‌صورتِ یک پوسته استوانه‌ای نازکِ کشسان درنظر گرفته شده‌است. معادله حاکم بر مُد تنفسیِ شعاعی با استفاده از اصل هامیلتون بدست آمده‌است. یک رابطه تحلیلی برای این بسامد بدست آمده‌است. مزیت این فرمول آن است که تابعیت بسامد مُد تنفسی شعاعی را نسبت به مشخصه‌های مکانیکی نانولوله‌کربنی تک‌لایه به‌وضوح نشان می‌دهد. این بررسی‌ها برای پیش‌بینیِ درست مشخصه‌های ارتعاشی نانولوله‌های‌کربنی تک‌لایه که کابردهای بالقوه‌ای در نانوکامپوزیت‌های حاویِ نانولوله، که به عنوان جاذب‌های صوتی استفاده می‌شوند، دارند. برای نشان دادن درستی نتایج، بسامدهای مُد تنفسی شعاعیِ ٤٠ نانولوله‌کربنی تک‌لایه در مطابقتی بسیار عالی با نتایج تجربیِ موجود با درصد خطایی کمتر از یک درصد بدست آمده‌است. همچنین بسامدهای مُد تنفسی شعاعیِ پیش‌بینی شده با مدل پوسته در این مقاله با نتایج بدست آمده توسط محققان دیگر بر اساس نظریه‌هایی همچون تابعیِ چگالی و نظریه کشسانی سه بعدی مقایسه شده‌اند. نتایج بدست‌آمده، کارآیی نظریه پوسته نازک را برای مدل‌سازیِ رفتار ارتعاشیِ بسامد مُد تنفسیِ شعاعی نانولوله‌کربنی تک‌لایه تأیید می‌کند.

doi: *10.5829/idosi.ije.2013.26.04a.13*